communications physics

A Nature Portfolio journal

Article

https://doi.org/10.1038/s42005-025-02113-1

Dissipation-induced non-equilibrium phases with temporal and spatial order

Zhao Zhang [1], Davide Dreon [1], Tilman Esslinger [1], Dieter Jaksch[2,3], Berislav Buca [3,4,5] ✉ & Tobias Donner [1]

Understanding spatial and temporal order in many-body systems is a key challenge, particularly in out-of-equilibrium settings. A major hurdle is developing controlled model systems to study these phases. We propose an experiment with a driven quantum gas coupled to a dissipative optical cavity, realizing a non-equilibrium phase diagram featuring both spatial and temporal order. The system's control parameter is the detuning between the drive frequency and cavity resonance. Negative detunings yield a spatially ordered phase, while positive detunings produce phases with both spatial order and persistent oscillations, forming dissipative spatio-temporal lattices. We also identify a phase where the dynamics dephase, leading to chaotic behavior. Numerical and analytical evidence supports these superradiant phases, showing that the spatio-temporal lattice originates from cavity dissipation. The atoms experience accelerated transport, either via uniform acceleration or abrupt momentum transitions. Our work provides insights into temporal phases of matter not possible at equilibrium.

Crystallization is usually understood as a phase transition, where a system of many particles at initially random positions self-arranges to acquire order in space[1]. Recently, the concept of temporal crystallization has also been introduced[2], where a system of many particles enters a state with repetitive motion, that is, order in time. Since space and time are the two fundamental continuous degrees of freedom required to describe nature and its evolution, spatial and temporal order are also the two types of fundamentally possible crystals.

Counter-intuitively, dissipation can be engineered to induce persistent oscillations and temporal crystallization in quantum systems, such that non-stationary states occur due to and not despite of dissipation[3–18]. A promising platform for realizing both spatial and temporal crystals is provided by hybrid quantum optical setups combining quantum gases with dissipative photonic systems[19–25]. Indeed, transitions to steady states of self-ordered crystals in space have been broadly explored[19,20,26], and both continuous[3,13,27–35] and discrete dissipative time crystals[36–40] have been recently identified as non-stationary states[6,31,41–48]. While so far, to the best of our knowledge, only systems featuring a single time crystalline phase have been considered, we here present a proposal for a dissipative system with a phase diagram featuring spatial order as well as different flavors of temporal order and also a transition to chaotic dynamics. The dissipation in our system not only induces the time-periodic behavior, but also leads to an acceleration of the self-ordered spatio-temporal crystal.

In our envisioned setup, a bosonic quantum gas is dispersively coupled with vacuum Rabi coupling strength g_0 to a dissipative optical cavity and pumped with a transverse laser field with Rabi frequency Ω_p (see Fig. 1). In contrast with most similar setups[26,41,42,49–51], we discuss a pure running-wave field instead of a standing-wave field, providing a continuous symmetry along the pump direction. Yet, dissipation given by photons leaking out of the cavity unbalances the forward and backward photon scattering processes, allowing for an acceleration of the atomic system. Since the laser frequency is far detuned by Δ_a from atomic resonance, the atoms act as scatterers at which photons from the pump field can be scattered into the cavity mode and vice versa. We consider a laser field detuned to a frequency higher than the atomic resonance, such that the atoms are expelled from regions with high intensities. In addition, opposite to the situation studied in[22], we consider a one-dimensional situation along the propagation direction of the pumping field, and the atoms are coupled to an antinode of the cavity field. This situation can be effectively realized using a λ-periodic lattice along the cavity axis, where λ is the wavelength of the driving laser field (see Supplementary Note 2). Employing the pumping strength $\eta_p = g_0\Omega_p/\Delta_a$ and the detuning $\Delta_c = \omega_p - \omega_c$ between the laser frequency ω_p and the cavity resonance ω_c as control parameters (with the dynamic dispersive shift[20] being absent in the considered one-dimensional situation), we map out the phase diagram, see Fig. 2. Besides the normal phase without spatial or temporal order, we predict for the pump-cavity red-detuned

[1]Institute for Quantum Electronics, Eidgenössische Technische Hochschule Zürich, Otto-Stern-Weg 1, CH-8093 Zurich, Switzerland. [2]Institut für Quantenphysik, Universität Hamburg, 22761 Hamburg, Germany. [3]Clarendon Laboratory, University of Oxford, Parks Road, Oxford, OX1 3PU, UK. [4]Université Paris-Saclay, CNRS, LPTMS, 91405 Orsay, France. [5]Niels Bohr International Academy, Niels Bohr Institute, Copenhagen University, Universitetsparken 5, 2100 Copenhagen, Denmark. ✉e-mail: berislav.buca@universite-paris-saclay.fr

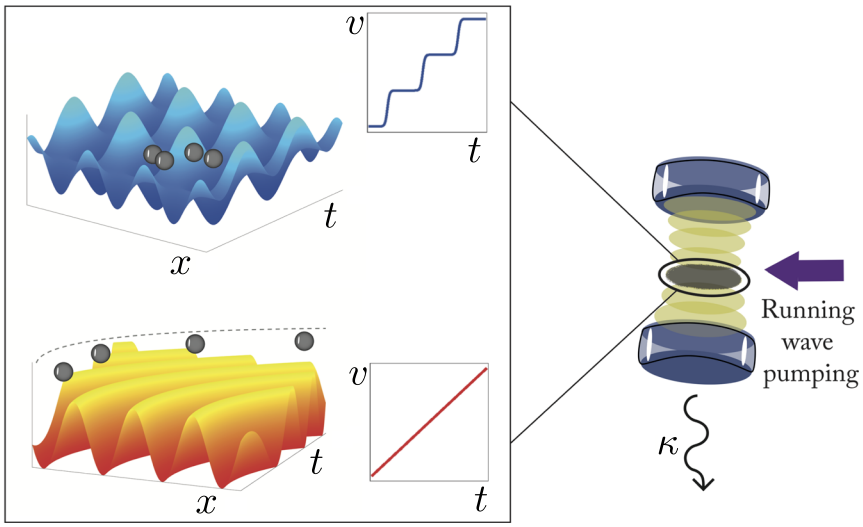

Fig. 1 | Setup. A running wave laser pumping a Bose-Einstein condensate coupled to a lossy optical cavity (right) induces a spatio-temporal lattice or a co-moving optical lattice (left). We consider dynamics in a one-dimensional system along the pump beam. The laser is blue-detuned with respect to the atomic resonance, providing a repulsive optical potential. Depending on the detuning between cavity and laser frequency, the system enters either a phase where the atoms constantly accelerate by a co-moving optical lattice (red), or a phase where they are pumped in a periodic fashion to increasingly higher momentum states, forming a spatio-temporal lattice (blue).

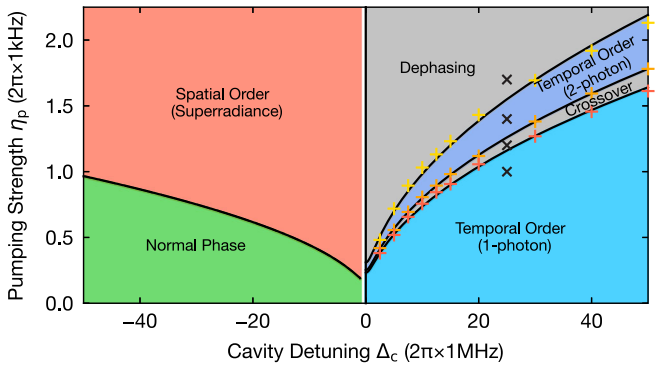

Fig. 2 | Dynamical phase diagram. For negative cavity detuning, the system leaves the normal phase (green) and enters a spatial lattice (red) above a threshold pump strength. For the absolute value of the detuning Δ_c being smaller than the dissipation rate κ, $|\Delta_c| \le \kappa$, the system shows incoherent dynamics (white). For positive cavity detunings, time dependent phases appear. Depending on the pumping strength η_p, the system shows temporal order in the single-photon or two-photon regime (blue) or dephasing regimes (gray). The colored crosses are obtained by a numerical simulation of the phase boundary, fixing Δ_c and scanning η_p. The black lines represent the phase boundary obtained by fitting these numerical simulation results with the function $\eta_p = b\sqrt{\Delta_c^2 + \kappa^2}$.

situation ($\Delta_c < 0$) the formation of a spatial lattice along the pump direction accompanied by a steady state of the cavity field. This spatial lattice is constantly accelerated along the pump direction, which leads to a running phase of the cavity field. For the pump-cavity blue-detuned regime ($\Delta_c > 0$), we predict for small pumping strengths the formation of a dissipative spatio-temporal lattice with an oscillating cavity field. For increasing pump strengths this regime crosses over into phases with modified temporal order displaying higher frequencies. For high enough pumping strengths, the cavity field oscillations dephase due to an increasing number of incommensurate frequencies that enter in the dynamics, giving rise to a chaotic region in the phase diagram.

All self-ordered phases are leading to an accelerated transport of the atoms[52] in the propagation direction of the pumping field. Generally, in the presence of a lattice and driving, one would expect Bloch oscillations[53] and no transport. However, the acceleration observed in our system is a result of momentum conservation in presence of cavity losses, and is proportional to the cavity field dissipation rate κ. Our results are given by mean-field theory, which we prove to be exact in the relevant parameter ranges and confirm with numerical simulations and a $SU(3)$ Holstein-Primakoff transformation.

Results

Driven Bose-Einstein condensate (BEC) in a dissipative cavity

We start our theoretical description with the time-dependent master equation in the frame rotating at the pumping laser frequency and eliminating the excited level of the atoms

$$\begin{aligned}\frac{d}{dt}\rho(t) &= \hat{\mathcal{L}}\rho(t)\\ &:= -i[H,\rho(t)] + \kappa[2a\rho(t)a^\dagger - \{a^\dagger a,\rho(t)\}]\end{aligned} \tag{1}$$

with

$$H/\hbar = -\Delta_c a^\dagger a + T_{\text{atom}} + \eta_p(a^\dagger O + aO^\dagger), \tag{2}$$

where a ($a^\dagger$) is the annihilation (creation) operator of a cavity photon and $T_{\text{atom}} = \sum_q \frac{\hbar q^2}{2m} c_q^\dagger c_q$ is the kinetic energy of the atoms. The operator $O = \sum_q c_{q+k}^\dagger c_q = \int dx \Psi^\dagger(x) e^{ikx} \Psi(x)$ characterizes the spatial overlap of the atomic field with the electric field of the pump laser with wave vector $k = 2\pi/\lambda$. Here, $\Psi(x)$ and c_q are the annihilation operators of an atom at position x and with momentum q, respectively. The expression $a^\dagger O$ captures the collective absorption of one recoil momentum $\hbar k$ of the atoms by scattering one photon from the pump field into the resonator, while $aO^\dagger$ describes the inverse process and both processes take place at the rate η_p. Since also cavity dissipation at rate κ leads to the annihilation of cavity photons, there is a net momentum transfer onto the atomic system in the direction of the propagation of the pumping field. In our one dimensional description, any momentum transfer in the direction of the cavity is neglected.

The equations of motion for the atomic momentum and cavity photon operators are

$$\begin{aligned} i\partial_t c_q &= \frac{\hbar q^2}{2m} c_q + \eta_p(a^\dagger c_{q-k} + a c_{q+k}),\\ i\partial_t a &= -(\Delta_c + i\kappa)a + \eta_p \sum_q c_{q+k}^\dagger c_q. \end{aligned} \tag{3}$$

We move to a mean-field description by replacing the operators with complex field amplitudes, $a \to \alpha = \langle a \rangle$ and $c_q \to \mathcal{C}_q = N\langle c_q \rangle$ and neglecting quantum fluctuations. The mean field equations of motion can

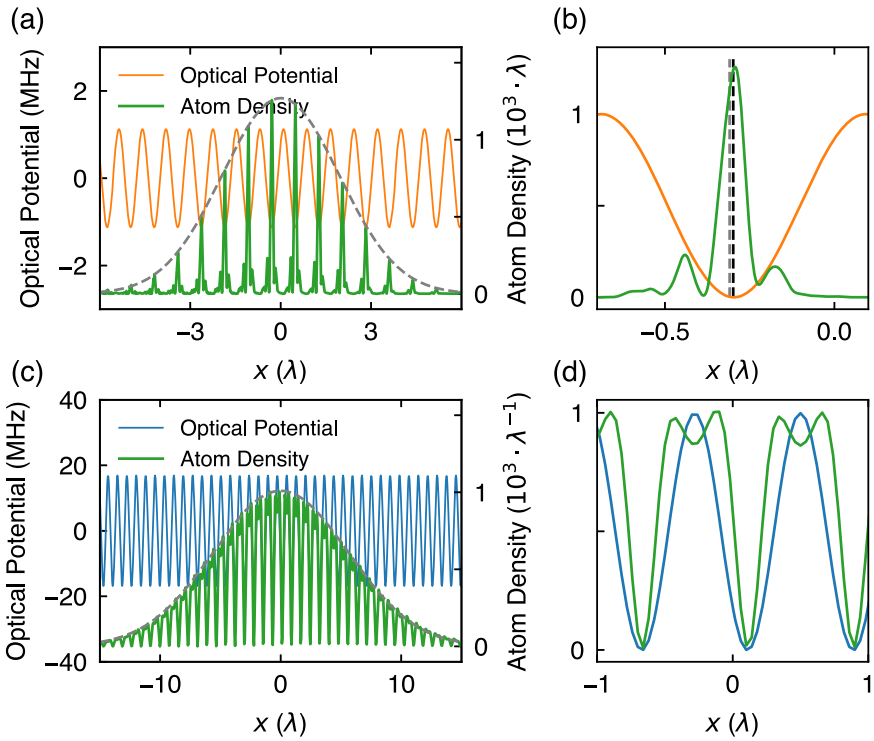

Fig. 3 | Optical potential and atomic wavefunctions for different detunings Δ_c. a, **b** In the red-detuned case ($\Delta_c = -2\pi \times 10$ MHz, driving $\eta_p = 2\pi \times 3.5$ kHz), the atomic wave function (green) localizes close to the minima of the optical potential (red). Non-zero cavity dissipation leads to a relative shift between the center of mass of the wave function (gray dashed line) and the minimum of the potential (black dashed line). **c**, **d** In the blue-detuned case ($\Delta_c = 2\pi \times 20$ MHz, $\eta_p = 2\pi \times 1$kHz), the additional phase shift by the cavity leads to an unstable situation where the atomic wave function localizes at the maxima of the optical potential. Subfigures (**c**) and (**d**) show a snapshot of the evolution where two momentum states are simultaneously populated and the optical potential becomes maximal. The subfigures (**b**) and (**d**) are closeups of subfigures (**a**) and (**c**), respectively (note the different axes).

also be written in real space equivalently,

$$\begin{aligned} i\partial_t \psi(x) &= -\frac{\hbar}{2m}\partial_x^2 \psi(x) + \eta_p(\alpha^* e^{ikx} + \alpha e^{-ikx})\psi(x) \\ i\partial_t \alpha &= -(\Delta_c + i\kappa)\alpha + \eta_p \int dx \psi^*(x) e^{ikx} \psi(x), \end{aligned} \tag{4}$$

where $\psi(x) = \langle \Psi(x) \rangle / \sqrt{N}$. The main results in this article are derived under this mean field approximation, whose validity can be proved with the atom-only master equation requiring η_p^2/κ to be smaller than all coupling rates (see Supplementary Note 3). Moreover, since the cavity field dynamics ($\kappa \sim$ MHz) is much faster than the time evolution of the atoms (given by the recoil frequency $\omega_r = \hbar k^2/(2m) \sim$ kHz), we adiabatically eliminate the photon mode: $\langle a \rangle = \frac{\eta_p}{\Delta_c + i\kappa} \langle O \rangle$, in analytical calculations later.

The atomic system scatters photons from the running wave pumping field into the optical cavity, which accordingly becomes populated with a coherent field. The interference between this field and the running wave pump field gives rise to a λ-periodic optical potential along the pump direction in which the atomic cloud orders in a self-consistent fashion[20]. Driving field and scattered field inside the cavity interfere destructively at the positions of the atoms, such that these are trapped in the local minima of the emerging optical potential. For red detuning ($\Delta_c < 0$) between the pump field and the cavity resonance, where the cavity field follows the drive field in phase, a steady state intra-cavity field can build up. In contrast for the blue-detuned case ($\Delta_c > 0$), an additional π phase shift between the driving and the scattered fields is introduced which gives rise to a non-stationary evolution. We separate the following discussion into the red and blue-detuned cases for Δ_c. We set $N = 10^5$ and $\kappa = 2\pi \times 1$ MHz for all numerical simulations, and assume properties of ^{87}Rb atoms.

In the following sections, we investigate the long-term dynamics of the system in the red-detuned ($\Delta_c < 0$) and blue-detuned ($\Delta_c > 0$) regime by numerically simulating the equations of motion Eq. (4) (see Methods), providing results in Figs. 3, 4 and 5. To intuitively understand the physical picture, we analytically study Eq. (4) in the red-detuned regime and Eq. (3) in the blue-detuned regime, while applying adiabatic elimination, providing an explanation for the numerical results.

Accelerating spatial lattice in the red-detuned regime

We start in the regime $\Delta_c < 0$ using a Bloch wave function modulated by an envelope function centered at x_0:

$$\psi(x) = f(x - x_0) e^{iqx} u_q(x - x_0), \tag{5}$$

as an ansatz solution of Eq. (4). Here, q is the quasi-momentum and $u_q(x)$ is an even, $\lambda -$ periodic function with its maximum located at $x = 0$. The slow-varying envelope function $f(x)$ satisfies $|(\partial_x f(x))/f(x)| \ll k$. We adiabatically eliminate the fast evolving cavity field and find the steady state cavity field amplitude α_0, as well as the optical potential generated by it:

$$V_o(x) = \eta_p N |\alpha_0| \cos\left[k(x - x_0) - \arg\left(\frac{1}{\Delta_c + i\kappa}\right)\right]. \tag{6}$$

For $\kappa = 0$, each Wannier component of the function $u_q(x)$ are localized at the minima of the self-consistent periodic potential, and both the cavity field and the density modulated atomic cloud are stationary.

However, for non-zero cavity dissipation, a phase shift $\delta = \tan^{-1}(\kappa/|\Delta_c|)$ is introduced, such that the maxima of the atomic wave function do not coincide with the minima of the self-generated optical potential, see Fig. 3b. This causes an effective force on the atomic wave packet and leads to transport in the $+x$ direction (see Supplementary Note 5),

$$\langle F \rangle = \left\langle \frac{dP}{dt} \right\rangle \approx \frac{\kappa \hbar k}{2} \frac{(N\eta_p)^2}{|\Delta_c|^2 + \kappa^2}, \tag{7}$$

where $P = \sum_q c_q^\dagger c_q q$ is the total momentum of all atoms. After building up the intra-cavity field, the periodic modulation of the atomic wave function and the self-generated potential leading to transport remain co-moving. Thus the force acting on the atomic system leads to a constant acceleration of the atomic cloud which preserves its periodic pattern. We show the time evolution of the atomic wave packet in real and in momentum space together with the cavity field amplitude in Fig. 4a. While the cavity field after self-organization stays approximately constant, the density modulated

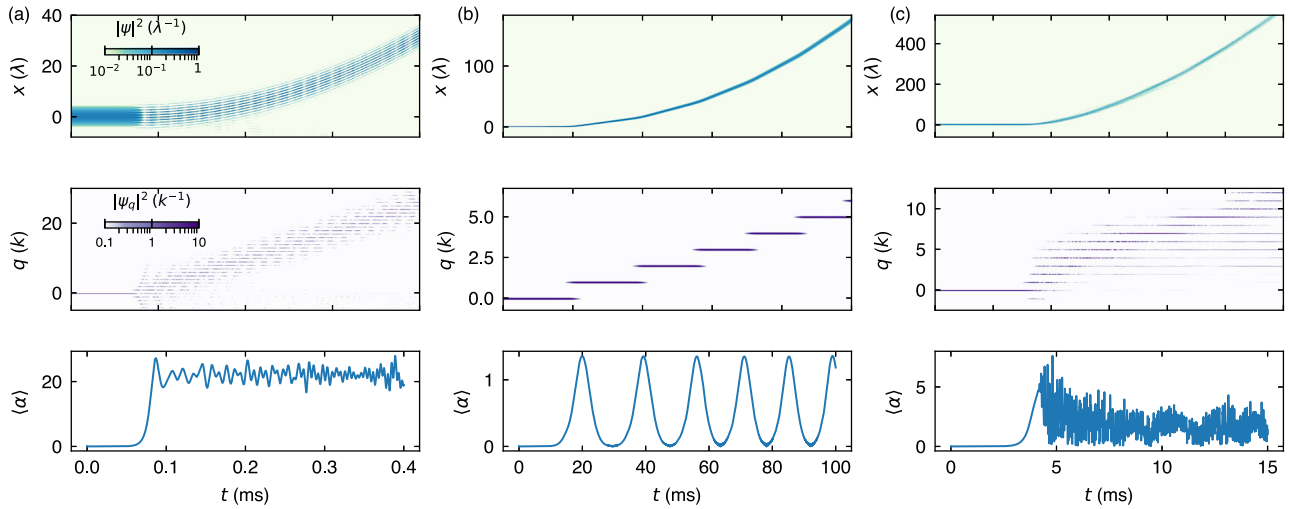

Fig. 4 | Time evolution of atoms and light. Time evolution of the atomic wave packet in real space (upper row) and in momentum space (middle row) together with the evolution of the mean cavity field amplitude (lowest row) in three different regimes. Note the different time scales for the different regimes. **a** Red-detuned regime (detuning $\Delta_c = -2\pi \times 10$ MHz, $\eta_p = 2\pi \times 3.5$ kHz). The atoms are continuously accelerated and the cavity is in a steady state. The wave function becomes repeatedly strongly localized at the potential minima but is properly normalized throughout the plot. **b** Blue-detuned regime with small pumping strengths η_p ($\Delta_c = 2\pi \times 20$MHz, $\eta_p = 2\pi \times 1$kHz). The atomic state is consecutively climbing up the momentum ladder in a step like fashion, driven by a cavity field that periodically switches on and off. **c** Blue-detuned regime with large pumping strengths η_p ($\Delta_c = 2\pi \times 10$ MHz, $\eta_p = 2\pi \times 1.5$ kHz). The strong driving strength induces simultaneous coupling to many momentum states which leads to a dephasing of the cavity field.

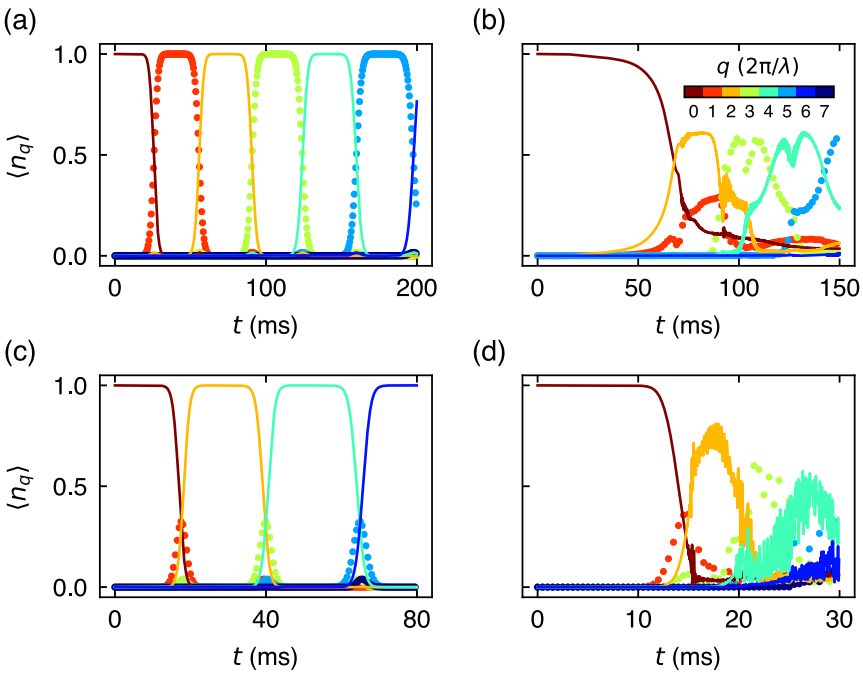

Fig. 5 | Momentum state populations. Time evolution of the momentum state populations $\langle n_q \rangle$ shown for the blue-detuned case $\Delta_c > 0$ in the one-photon regime (**a**), the dephased regime at intermediate driving η_p (**b**), the two-photon regime (**c**), and the dephased regime at high η_p (**d**). All odd momentum states are plotted in dotted lines. The parameters for these situations are indicated by black crosses in Fig. 2.

cloud is accelerated, and correspondingly higher momentum states are occupied. Very close to cavity resonance ($\Delta_c \sim \kappa$), the phase shift δ induces incoherent dynamics for $\Delta_c < 0$, as indicated by the white region in the phase diagram, see Fig. 2. Since we assume the cavity dissipation to be much larger than the recoil energy, this incoherent dynamics appearing close to $\Delta_c = 0$ dominates over effects of the dynamic detuning of the scattered light due to the acceleration of the atoms.

Dissipative spatio-temporal lattice in the blue-detuned regime

For blue detuning between pump frequency and cavity resonance ($\Delta_c > 0$), the cavity field acquires an additional π phase shift. The atomic Bloch wave packet in the emerging periodic potential thus becomes unstable, see Fig. 3d. Each Wannier component of the atomic wave function now tries to localize at the maxima of the optical potential and no stationary state is formed, hence the previous description fails. Instead of applying ansatz Eq. (5) in real space, we work in the momentum space and choose all N atoms to be initially in the momentum state $|q\rangle$, which is only coupled to the neighboring momentum states $|q-k\rangle$ and $|q+k\rangle$. Assuming a discretized momentum space is well justified since the initial state is a BEC and further momentum states can only be occupied via photon scattering processes. The dissipation suppresses the transition $|q\rangle \to |q-k\rangle$ and only the $|q\rangle \to |q+k\rangle$ transition is allowed in the short time dynamics in the blue-detuned regime (see Supplementary Note 7). This ensures that in the blue-detuned regime ($\Delta_c > 0$), the atoms accelerate in $+x$ direction.

To gain some insight into the dynamics we first truncate the dynamics accordingly to only two neighboring momentum states and write the equations of motion for the states $|q\rangle$ and $|q+k\rangle$

$$i\partial_t \begin{pmatrix} \mathcal{C}_q \\ \mathcal{C}_{q+k} \end{pmatrix} = \begin{pmatrix} \omega_q & \eta_\mathrm{p}\alpha \\ \eta_\mathrm{p}\alpha^* & \omega_{q+k} \end{pmatrix} \begin{pmatrix} \mathcal{C}_q \\ \mathcal{C}_{q+k} \end{pmatrix}, \tag{8}$$

where $\omega_q = \hbar q^2/(2m)$ is the frequency corresponding to the atomic kinetic energy with momentum $\hbar q$. The cavity field amplitude $\alpha = \frac{N\eta_\mathrm{p}}{\Delta_\mathrm{c}+i\kappa}\mathcal{C}^*_{q+k}\mathcal{C}_q$ depends on the product of the amplitudes of the two involved momentum states according to the adiabatic elimination. A finite initial occupation of the state $|q+k\rangle$ is ensured in our simulation due to the finite size of the chosen wave packet. In addition, due to the dissipative character of the system only the state $|q+k\rangle$ experiences gain, while the transitions to $|q-k\rangle$ are suppressed. In this 2-level system, $\eta_\mathrm{p}\alpha$ is the coupling depends on the amplitude of both levels. Once all population are driven from $|q\rangle$ to $|q+k\rangle$ the occupation of the $|q\rangle$ state drops to zero and the driving accordingly turns off. Now, the $|q+k\rangle$ state is macroscopically occupied and a new cycle of transition between the states $|q+k\rangle$ and $|q+2k\rangle$ begins while dissipation again prevents a return to lower momentum states. The simulated occupation of momentum states according to Eq. (3) is shown in Fig. 5a. The atoms accelerate in a step-like fashion, while the cavity field evolves periodically. The field is populated only during the transitions between neighboring momentum states and vanishes when one momentum state is fully occupied by all atoms, see Fig. 4b. The atomic cloud is periodically changing its shape while atoms simultaneously populate two different momentum states. We hence dub this non-stationary phase of the system a dissipative spatio-temporal lattice. The truncation to two momentum states fails for the red-detuned case, where always several momentum states are occupied, see Fig. 4a.

The energy spacing between two neighboring momentum states is given by the recoil energy and momenta as $\hbar\omega_\mathrm{r}(2q/k+1)$. Moving away from the weak coupling limit $\eta_\mathrm{p}\alpha(t) \leq \frac{N\eta_\mathrm{p}^2}{4|\Delta_\mathrm{c}+i\kappa|} \ll \omega_\mathrm{r}$ by either applying a strong pump η_p or a small cavity detuning Δ_c, also transitions to non-neighboring momentum states can be induced, as characterized by the parameter

$$b = \frac{N\eta_\mathrm{p}^2}{4\omega_\mathrm{r}|\Delta_\mathrm{c}+i\kappa|}, \tag{9}$$

which also has been used in Fig. 2 for the regime $\Delta_\mathrm{c} > 0$.

If such transitions become relevant, a truncation of the momentum basis fails and we study the system numerically instead by evolving equations (3). We observe that for sufficiently strong pumping η_p processes set in where the atoms absorb two photons and accordingly gain $2\hbar k$ momentum in each cycle of the cavity evolution, as shown in Fig. 5c. For even stronger pump rates, additional frequency components emerge and cause a dephasing of the cavity field such that the oscillatory behavior breaks down. In this situation the dissipative spatio-temporal lattice disappears and a phase with a dephased cavity field and simultaneous occupation of multiple momentum states with increasing momenta emerges, see Fig. 4c and 5d. Such a dephased region also appears as a narrow stripe between the single-photon and the two-photon phases. Its time evolution is shown in Fig. 5b. The transition to these dephased regions can be explained by a leakage of the population out of a few-mode model: Assume that the initial population in two neighboring modes is $\langle n_q\rangle = 1-\epsilon$ and $\langle n_{q+k}\rangle = \epsilon$. When most of the atoms are transferred from mode q to $q+k$, for strong enough pumping a fraction ϵ' of the atoms might already populate the next mode $q+2k$. If $\epsilon' > \epsilon$, this leakage will become more severe after each cycle of the cavity field oscillation and thus the temporal order is not stable. This condition gives the phase boundary between the one-photon spatial-temporal lattice phase and the crossover area. Exploring the nature of the transition between the one-photon and two-photon temporal order is intriguing but goes beyond our approach.

Transitions between phases with different sign of Δ_c

We studied the phase diagram additionally (see Methods) by mapping the full model to a three-level Dicke-like model[54–57]. While such an analytical approach cannot elucidate the spatial nature of the phases—which we instead captured using numerical simulations—it predicts in the large κ limit a phase transition at the critical line $\Delta_\mathrm{c} = 0$, and diverging modes in all phases. By contrast, for $\kappa = 0$ the analytical model reduces to a set of equations identical to those for the standard two-level Dicke model[24] further confirming that the (spatio)-temporal order is dissipation induced. However, this three-mode approximation is not sufficient to capture the full long-time dynamics leading to the accelerated transport in all regimes. In particular, it cannot capture the dephasing regime, which occurs due to the interference of a very large number of momentum modes with incommensurate frequencies.

The phase transitions crossing the critical line $\Delta_\mathrm{c} = 0$ can also be explained semi-classically as disappearance of a stable potential minimum. The potential energy that atoms experience in the accelerated frame is the sum of the self-organized optical lattice potential (Eq. (6)) and the linear potential from the inertial force (Eq. (7)):

$$V(x) = V_o(x) + \left\langle \frac{dP}{dt} \right\rangle x. \tag{10}$$

In the red-detuned regime, the extremal position x_ex of the potential in each lattice cell is a stable point with $d^2V(x_\mathrm{ex})/dx^2 > 0$. Thus, the Wannier component of the atomic wavefunction in each lattice well stays at the minimum and spatial order forms. Crossing the boundary line $\Delta_\mathrm{c} = 0$, this minimum x_ex turns into an inflection point of the potential ($d^2V(x_\mathrm{ex})/dx^2 = 0$) and the system experiences a phase transition towards the blue-detuned regime ($\Delta_\mathrm{c} > 0$), where the extremum becomes the maximum point of the potential energy ($d^2V(x_\mathrm{ex})/dx^2 < 0$). Therefore, the Bloch wavefunction ansatz Eq. (5) is not stable anymore, and the spatial order breaks down. Similar to the Dicke model, and due to the infinite range character of the interactions, this phase transition is captured by a mean field, with the transition induced by the cavity[58]. A similar transition between red- and blue detuned regimes has already been observed in a ring cavity, where the redistribution of photons between two counter propagating modes can lead to an acceleration[59]. That study however was limited to the situation $\Delta_\mathrm{a} < 0$ of attractive light forces, where the time dynamics we discuss is absent.

Discussion

Many-body cavity QED setups with running wave drives have already been realized[60,61], however so far only with red-detuned light fields. For an experimental implementation of our model currently available setups[26,43,49,60,61] would additionally require confinement of the atoms in a λ-spaced lattice along the y-direction. The described phenomena should be observable both via a heterodyne measurement of the field leaking from the cavity providing access to the phase and the amplitude, as well as via time of flight images of the atomic system revealing the occupied momentum states or via atomic images in real space directly reflecting the transport of atoms. Specifically the real-time access to the light field would provide deep insight into the dynamics of the system. One could, for example, use the Fourier transform of the field amplitude $\alpha(t)$ as order parameter to distinguish the different phases.

Due to the finite extent of the cavity mode, the atoms will be eventually transported out of the coupling region of the cavity, limiting the accessible time evolution. However, the fundamental processes and phases described in this work should be well observable (see Supplementary Note 2). In this work, we neglected the influence of atomic collisional interactions, which we expect however to only lead to small shifts of the transition lines for typical atomic densities.

Our work opens theoretical and experimental possibilities for studying novel quantum optical phases far from equilibrium. It is an interesting question to identify if there are universal principles governing the coexistence of spatial and temporal order in the same system, and to gain a deeper understanding of processes breaking spatial translational and time translational orders. Furthermore such a system may host unique quasiparticles or collective excitations due to the interaction between spatial and temporal ordering. Although our approach is exact in the weakly-interacting limit, which is perfectly valid for the system studied, an interesting theoretical question is if the persistent oscillations in the dissipative spatio-temporal lattice survive interactions between the atoms. This, along with the influence of quantum fluctuations (beyond mean-field effects), could be studied in the strong dissipation limit analogously to[27] using the theory of dynamical symmetries[3,62], i.e., order-by-order in inverse powers of κ allowing for incorporating quantum fluctuations (and finite-size effects) fully. Studying the model in this way could demonstrate formation of non-trivial entanglement in the system. Interactions between the atoms could similarly induce synchronization inside the lattice along the proposals in[3,63,64].

Methods

We here provide an overview of the different numerical and analytical approaches we applied in this work. Detailed derivations are shown in the SI.

Starting point for our numerical and analytical study is a mean-field simulation of the Hamiltonian in Eq. (2) in real space, while the atomic field and the cavity photon amplitude are governed by the equation of motion:

$$\begin{aligned} i\partial_t\psi(x) = &-\frac{\hbar}{2m}\partial_x^2\psi(x) + \eta_\mathrm{p}(a^\dagger + a)\cos(kx)\psi(x) \\ &+ i\,\eta_\mathrm{p}(a^\dagger - a)\sin(kx)\psi(x), \end{aligned} \tag{11}$$

$$\begin{aligned} i\partial_t a = &-\Delta_\mathrm{c} a + \eta_\mathrm{p}\int dx\psi^\dagger(x)\cos(kx)\psi(x) \\ &+ i\eta_\mathrm{p}\int dx\psi^\dagger(x)\sin(kx)\psi(x) - i\kappa a. \end{aligned} \tag{12}$$

By numerically solving these equations of motion, we obtain the phase diagram in Fig. 2, as well as the dynamics of the atoms and the cavity photon amplitude in the different phases (Fig. 4). Based on the ansatz solution for this equation of motion (Eq. (4)), we derive the acceleration of the spatial lattice in the red-detuned regime. In addition, it captures the phase transition between spatial order and dephasing.

To get a better intuition for the temporally ordered phase and its breakdown under increased pumping, we restrict the equations of motion to discrete momentum modes:

$$i\partial_t c_q = \frac{\hbar q^2}{2m}c_q + \eta_\mathrm{p}(a^\dagger c_{q-k} + a c_{q+k}), \tag{13}$$

$$i\partial_t a = -(\Delta_\mathrm{c} + i\kappa)a + \eta_\mathrm{p}\sum_q c^\dagger_{q+k}c_q. \tag{14}$$

where the momentum q is an integer times the recoil momentum k. The validity of these equations of motion for discrete momenta is verified numerically. By truncating the equation of motion to two and three modes, we explain analytically the dynamics of the temporal order (Eq. (7)) as well as the breakdown of the temporal order (Eq. S27).

Based on the truncated model on the discrete momentum modes, we also go beyond the mean-field approximation by studying quantum fluctuations in a three-level Dicke-like model.

The Three-level Dicke-like model

We begin by taking the Hamiltonian from the main text,

$$H = -\hbar\Delta_\mathrm{c}a^\dagger a + \sum_q \hbar\omega_q c_q^\dagger c_q + \eta_\mathrm{p}\left(a^\dagger\left[\sum_q c^\dagger_{q+k}c_q\right] + h.c.\right). \tag{15}$$

We reduce to the three mode approximation, i.e., we keep only the $c_1 := c_q$ and $c_2 := c_{q+k}, c_3 := c_{q-k}$ modes in the Hamiltonian. We may then perform a $SU(3)$ Schwinger boson mapping[54], $S^+_{12} = c_2^\dagger c_1$, $S^+_{13} = c_3^\dagger c_1$, $S^-_\mu = (S^+_\mu)^\dagger$, $S^z_{12} = c_2^\dagger c_2 - c_3^\dagger c_3 - c_1^\dagger c_1$, $S^z_{13} = c_3^\dagger c_3 - c_2^\dagger c_2 - c_1^\dagger c_1$, which obeys the $SU(3)$ algebra with representation N[54,65] enforcing the total atom number $N = c_3^\dagger c_3 + c_2^\dagger c_2 + c_1^\dagger c_1$. This allows us to rewrite the model, up to an irrelevant constant $N\omega_q$, in terms of a three-level Dicke-like one,

$$H/\hbar = \omega_0(S^z_{12} + S^z_{13}) - \Delta_\mathrm{c}a^\dagger a + \eta_\mathrm{p}\left(a^\dagger(S^+_{12} + S^-_{13}) + h.c.\right), \tag{16}$$

where $\omega_0 = \frac{\omega_{q+k} - \omega_q}{2}$. We now switch to the large atom number limit $N \to \infty$ and perform a generalized Holstein-Primakoff transformation[54,66] to obtain,

$$H/\hbar = \omega_0(N_{12} + N_{13}) - \Delta_\mathrm{c}a^\dagger a + \eta_\mathrm{p}\left(a^\dagger(a^\dagger_{12} + a_{13}) + h.c.\right), \tag{17}$$

where we defined a_x to be bosonic operators and $N_x = a_x^\dagger a_x$. The full model including the Lindblad jump operator is now quadratic and may be exactly solved[67,68]. It is simplest to write the equations of motion for one-point functions $\vec{v} = \{\langle a\rangle, \langle a\rangle^*, \langle a_{12}\rangle, \langle a_{12}\rangle^*, \langle a_{13}\rangle, \langle a_{13}\rangle^*\}$. These equations, of course, close into a set of six equations. Using Eq. (1) we may find,

$$\frac{d\vec{v}}{dt} = \mathcal{M}\vec{v}, \tag{18}$$

where,

$$\mathcal{M} = \begin{pmatrix} i\Delta_c - \kappa & 0 & 0 & i\eta_p & -i\eta_p & 0 \\ 0 & -\kappa - i\Delta_c & -i\eta_p & 0 & 0 & i\eta_p \\ 0 & i\eta_p & -i\omega_0 & 0 & 0 & 0 \\ -i\eta_p & 0 & 0 & i\omega_0 & 0 & 0 \\ -i\eta_p & 0 & 0 & 0 & -i\omega_0 & 0 \\ 0 & i\eta_p & 0 & 0 & 0 & i\omega_0 \end{pmatrix} \tag{19}$$

The eigenvalue equation $\det(\mathcal{M} - \Lambda) = 0$ for this matrix is

$$\begin{aligned} &\Delta_c^2\left(\Lambda^2 + \omega_0^2\right)^2 + 4\omega_0\Delta_c\left(\Lambda^2 + \omega_0^2\right)\eta_p^2 \\ &+ (\kappa + \Lambda)^2\left(\Lambda^2 + \omega_0^2\right)^2 + 4\omega_0^2\eta_\mathrm{p}^4 = 0 \end{aligned} \tag{20}$$

Assuming $\kappa \to \infty$ as the experimentally relevant bad cavity limit, we expand this equation in $1/\kappa$. We always have two eigenvalues with positive real part (depending on the sign of Δ_c) $\Lambda_\mathrm{div} = \{\frac{1}{6}\left(\sqrt{3} + i\right)\Delta_c, \frac{1}{6}\left(-\sqrt{3} + i\right)\Delta_c\}$ implying that the model is always unstable. This is consistent with the numerics which implies that we cannot truncate to a finite number of modes in the long-time limit. However, we also see that at the point $\Delta_c = 0$ the two unstable solutions interchange signaling the phase transition between the red and blue-detuned regime from the numerical study in the main text. This also suggests that the phase transition is a manifestation of quantum Zeno dynamics[69,70]. Indeed, setting $\kappa = 0$, by looking at the linear stability analysis of the trivial normal phase[57], we find a standard Dicke phase transition between a normal and superradiant phase, further confirming the dissipation-induced nature of our spatio-temporal lattice. Crucially, in our model, due to the mapping at momenta q and $q + k$, the oscillations are accompanied by the formation of a spatial lattice, as well as a temporal one (persistent oscillations).

Data availability

The data displayed in the figures of this study are available in the data repository of ETH Zurich's Research Collection (https://doi.org/10.3929/ethz-b-000731562).

Received: 16 August 2024; Accepted: 28 April 2025;
Published online: 22 May 2025

References

1. Cardy, J. Scaling and Renormalization in Statistical Physics, Cambridge Lecture Notes in Physics (Cambridge University Press, 1996).
2. Wilczek, F. Quantum time crystals. *Phys. Rev. Lett.* **109**, 160401 (2012).
3. Buča, B., Tindall, J. & Jaksch, D. Non-stationary coherent quantum many-body dynamics through dissipation. *Nat. Commun.* **10**, 1730 (2019).
4. Booker, C., Buča, B. & Jaksch, D. Non-stationarity and dissipative time crystals: spectral properties and finite-size effects. *N. J. Phys.* **22**, 085007 (2020).
5. Barberena, D., Lewis-Swan, R. J., Thompson, J. K. & Rey, A. M. Driven-dissipative quantum dynamics in ultra-long-lived dipoles in an optical cavity. *Phys. Rev. A* **99**, 053411 (2019).
6. Dogra, N. et al. Dissipation-induced structural instability and chiral dynamics in a quantum gas. *Science* **366**, 1496 (2019).
7. Scarlatella, O., Fazio, R. & Schiró, M. Emergent finite frequency criticality of driven-dissipative correlated lattice bosons. *Phys. Rev. B* **99**, 064511 (2019).
8. Chiacchio, E. I. R. & Nunnenkamp, A. Dissipation-induced instabilities of a spinor bose-einstein condensate inside an optical cavity. *Phys. Rev. Lett.* **122**, 193605 (2019).
9. Seibold, K., Rota, R. & Savona, V. Dissipative time crystal in an asymmetric nonlinear photonic dimer. *Phys. Rev. A* **101**, 033839 (2020).
10. Oberreiter, L., Seifert, U. & Barato, A. C. Stochastic discrete time crystals: Entropy production and subharmonic synchronization. *Phys. Rev. Lett.* **126**, 020603 (2021).
11. Mendoza-Arenas, J. J. & Buča, B. Self-induced entanglement resonance in a disordered bose-fermi mixture (2021), arXiv:2106.06277 [cond-mat.quant-gas].
12. Minganti, F., Arkhipov, I. I., Miranowicz, A. & Nori, F. Correspondence between dissipative phase transitions of light and time crystals (2020), arXiv:2008.08075 [quant-ph].
13. Carollo, F. & Lesanovsky, I. Exact solution of a boundary time-crystal phase transition: time-translation symmetry breaking and non-markovian dynamics of correlations. *Phys. Rev. A* **105**, L040202 (2022).
14. Seetharam, K., Lerose, A., Fazio, R. & Marino, J. Correlation engineering via nonlocal dissipation. *Phys. Rev. Res.* **4**, 013089 (2022).
15. Chen, Y. & Navarrete-Benlloch, C. Collectively pair-driven-dissipative bosonic arrays: exotic and self-oscillatory condensates (2021), arXiv:2111.07326 [cond-mat.quant-gas].
16. Seibold, K., Rota, R., Minganti, F. & Savona, V. Quantum dynamics of dissipative kerr solitons. *Phys. Rev. A* **105**, 053530 (2022).
17. Iemini, F. et al. Boundary time crystals. *Phys. Rev. Lett.* **121**, 035301 (2018).
18. Sarkar, S. & Dubi, Y. Signatures of discrete time-crystallinity in transport through an open fermionic chain. *Commun. Phys.* **5**, 155 (2022).
19. Ritsch, H., Domokos, P., Brennecke, F. & Esslinger, T. Cold atoms in cavity-generated dynamical optical potentials. *Rev. Mod. Phys.* **85**, 553 (2013).
20. Farokh Mivehvar, T. D., Piazza, F. & Ritsch, H. Cavity qed with quantum gases: new paradigms in many-body physics. *Adv. Phys.* **70**, 1 (2021).
21. Lin, R. et al. Dissipation-engineered family of nearly dark states in many-body cavity-atom systems. *Phys. Rev. Lett.* **128**, 153601 (2022).
22. Piazza, F. & Ritsch, H. Self-ordered limit cycles, chaos, and phase slippage with a superfluid inside an optical resonator. *Phys. Rev. Lett.* **115**, 163601 (2015).
23. Alaeian, H., Soriente, M., Najafi, K. & Yelin, S. F. Noise-resilient phase transitions and limit-cycles in coupled kerr oscillators (2024).
24. Keeling, J., Bhaseen, M. J. & Simons, B. D. Collective dynamics of bose-einstein condensates in optical cavities. *Phys. Rev. Lett.* **105**, 043001 (2010).
25. Bhaseen, M. J., Mayoh, J., Simons, B. D. & Keeling, J. Dynamics of nonequilibrium dicke models. *Phys. Rev. A* **85**, 013817 (2012).
26. Baumann, K., Guerlin, C., Brennecke, F. & Esslinger, T. Dicke quantum phase transition with a superfluid gas in an optical cavity. *Nature* **464**, 1301 (2010).
27. Buča, B. & Jaksch, D. Dissipation induced nonstationarity in a quantum gas. *Phys. Rev. Lett.* **123**, 260401 (2019).
28. Lledó, C., Mavrogordatos, T. K. & Szymańska, M. H. Driven bose-hubbard dimer under nonlocal dissipation: a bistable time crystal. *Phys. Rev. B* **100**, 054303 (2019).
29. Daviet, R., Zelle, C. P., Rosch, A. & Diehl, S. Nonequilibrium criticality at the onset of time-crystalline order. *Phys. Rev. Lett.* **132**, 167102 (2024).
30. Wu, X. et al. Dissipative time crystal in a strongly interacting rydberg gas. *Nat. Phys.* **20**, https://doi.org/10.1038/s41567-024-02542-9 (2024).
31. Halati, C.-M., Sheikhan, A., Morigi, G. & Kollath, C. Controlling the dynamics of atomic correlations via the coupling to a dissipative cavity (2024), arXiv:2403.20096 [cond-mat.quant-gas].
32. Mattes, R., Lesanovsky, I. & Carollo, F. Entangled time-crystal phase in an open quantum light-matter system. *Phys. Rev. A* **108**, https://doi.org/10.1103/physreva.108.062216 (2023).
33. Carollo, F., Lesanovsky, I., Antezza, M. & Chiara, G. D. Quantum thermodynamics of boundary time-crystals. *Quantum Sci. Technol.* **9**, 035024 (2024).
34. Nakanishi, Y., Hanai, R., & Sasamoto, T. Continuous time crystals as a pt symmetric state and the emergence of critical exceptional points (2024), arXiv:2406.09018.
35. Heugel, T. L., Eichler, A., Chitra, R. & Zilberberg, O. The role of fluctuations in quantum and classical time crystals. *SciPost Phys. Core* **6**, 053 (2023).
36. Tucker, K. et al. Shattered time: can a dissipative time crystal survive many-body correlations? *N. J. Phys.* **20**, 123003 (2018).
37. Zhu, B., Marino, J., Yao, N. Y., Lukin, M. D. & Demler, E. A. Dicke time crystals in driven-dissipative quantum many-body systems. *N. J. Phys.* **21**, 073028 (2019).
38. Chinzei, K. & Ikeda, T. N. Time crystals protected by floquet dynamical symmetry in hubbard models. *Phys. Rev. Lett.* **125**, 060601 (2020).
39. Cosme, J. G., Skulte, J. & Mathey, L. Time crystals in a shaken atom-cavity system. *Phys. Rev. A* **100**, 053615 (2019).
40. Zaletel, M. P. et al. Colloquium: quantum and classical discrete time crystals. *Rev. Mod. Phys.* **95**, 031001 (2023).
41. Keßler, H. et al. Observation of a dissipative time crystal. *Phys. Rev. Lett.* **127**, 043602 (2021).
42. Kongkhambut, P. et al. Observation of a continuous time crystal. *Science* **377**, 670 (2022).
43. Dreon, D. et al. Self-oscillating pump in a topological dissipative atom-cavity system. *Nature* **608**, 494 (2022).
44. Taheri, H., Matsko, A. B., Maleki, L. & Sacha, K. All-optical dissipative discrete time crystals. *Nat. Commun.* **13**, 848 (2022).

45. Li, Y., Li, X. & Jin, J. Quantum nonstationary phenomena of spin systems in collision models. *Phys. Rev. A* **107**, 042205 (2023).
46. Li, X., Li, Y. & Jin, J. Synchronization of persistent oscillations in spin systems with nonlocal dissipation. *Phys. Rev. A* **107**, 032219 (2023).
47. Wang, H. & Wang, J. Time-crystal phase emerging from a qubit network under unitary random operations. *Phys. Rev. A* **108**, 012209 (2023).
48. Eckseler, J. & Schnack, J. Flatband makes the wave go round (2024), arXiv:2404.18646 [cond-mat.str-el].
49. Klinder, J., Keßler, H., Wolke, M., Mathey, L. & Hemmerich, A. Dynamical phase transition in the open dicke model. *Proc. Natl. Acad. Sci. USA* **112**, 3290 (2015).
50. Kollár, A. J. et al. Supermode-density-wave-polariton condensation with a bose-einstein condensate in a multimode cavity. *Nat. Commun.* **8**, https://doi.org/10.1038/ncomms14386 (2017).
51. Zhang, X. et al. Observation of a superradiant quantum phase transition in an intracavity degenerate Fermi gas. *Science* **373**, 1359 (2021).
52. Zheng, W. & Cooper, N. R. Anomalous diffusion in a dynamical optical lattice. *Phys. Rev. A* **97**, 021601 (2018).
53. Meinert, F. et al. Bloch oscillations in the absence of a lattice. *Science* **356**, 945 (2017).
54. Skulte, J. et al. Parametrically driven dissipative three-level dicke model. *Phys. Rev. A* **104**, https://doi.org/10.1103/physreva.104.063705 (2021).
55. Cola, M. M., Bigerni, D. & Piovella, N. Recoil-induced subradiance in an ultracold atomic gas. *Phys. Rev. A* **79**, 053622 (2009).
56. Fan, J., Chen, G. & Jia, S. Atomic self-organization emerging from tunable quadrature coupling. *Phys. Rev. A* **101**, https://doi.org/10.1103/physreva.101.063627 (2020).
57. Kirton, P., Roses, M. M., Keeling, J. & Dalla Torre, E. G. Introduction to the dicke model: from equilibrium to nonequilibrium, and vice versa. *Adv. Quantum Technol.* **2**, 1800043 (2018).
58. Strack, P. & Sachdev, S. Dicke quantum spin glass of atoms and photons. *Phys. Rev. Lett.* **107**, 277202 (2011).
59. Schmidt, D., Tomczyk, H., Slama, S. & Zimmermann, C. Dynamical instability of a bose-einstein condensate in an optical ring resonator. *Phys. Rev. Lett.* **112**, 115302 (2014).
60. Arnold, K. J., Baden, M. P. & Barrett, M. D. Self-organization threshold scaling for thermal atoms coupled to a cavity. *Phys. Rev. Lett.* **109**, 153002 (2012).
61. Vaidya, V. D. et al. Tunable-range, photon-mediated atomic interactions in multimode cavity qed. *Phys. Rev. X* **8**, 011002 (2018).
62. Buča, B. Out-of-time-ordered crystals and fragmentation. *Phys. Rev. Lett.* **128**, 100601 (2022).
63. Tindall, J., Sánchez Muñoz, C., Buča, B. & Jaksch, D. Quantum synchronisation enabled by dynamical symmetries and dissipation. *N. J. Phys.* **22**, 013026 (2020).
64. Buca, B., Booker, C. & Jaksch, D. Algebraic theory of quantum synchronization and limit cycles under dissipation. *SciPost Phys.* **12**, https://doi.org/10.21468/scipostphys.12.3.097 (2022).
65. Lacroix, C., Mendels, P. & Mila, F. Introduction to frustrated magnetism: materials, experiments, theory, Vol. 164 (Springer Science & Business Media, 2011).
66. Wagner, M. A nonlinear transformation of su (3)-spin-operators to bosonic operators. *Phys. Lett. A* **53**, 1 (1975).
67. Prosen, T. Third quantization: a general method to solve master equations for quadratic open fermi systems. *N. J. Phys.* **10**, 043026 (2008).
68. Prosen, T. & Seligman, T. H. https://doi.org/10.1088/1751-8113/43/39/392004 Quantization over boson operator spaces (2010).
69. Fröml, H., Muckel, C., Kollath, C., Chiocchetta, A. & Diehl, S. Ultracold quantum wires with localized losses: Many-body quantum zeno effect. *Phys. Rev. B* **101**, 144301 (2020).
70. Bezvershenko, A. V., Halati, C.-M., Sheikhan, A., Kollath, C. & Rosch, A. Dicke transition in open many-body systems determined by fluctuation effects. *Phys. Rev. Lett.* **127**, 173606 (2021).

Acknowledgements

We thank V. Jukić Buča for help with Fig. 1, and Alexander Baumgärtner and Simon Hertlein for useful discussions. This work is supported by the Cluster of Excellence 'CUI: Advanced Imaging of Matter' of the Deutsche Forschungsgemeinschaft (DFG) - EXC 2056 - project ID 390715994, EPSRC programme grants EP/P009565/1, EP/P01058X/1, EPSRC National Quantum Technology Hub in Networked Quantum Information Technology (EP/M013243/1), the SNF projects 182650, 175329 (NAQUAS QuantERA), IZBRZ2 186312, NCCR QSIT, 217124, 223274, 221538, the French National Research Agency (ANR) under project ANR-24-CPJ1-0150-01, and by a research grant (42085) from VILLUM FONDEN. We further acknowledge funding from from the Swiss State Secretariat for Education, Research and Innovation (SERI) (MB22.00090).

Author contributions

Z.Z. and D.D. performed numerical simulations. Z.Z. and B.B. provided analytical solutions. T.E., D.J., and T.D. supervised the work. All authors contributed to the interpretation of the data and the writing of the manuscript.

Competing interests

The authors declare no competing interest.

Additional information

Supplementary information The online version contains supplementary material available at https://doi.org/10.1038/s42005-025-02113-1.

Correspondence and requests for materials should be addressed to Berislav Buca.

Peer review information *Communications Physics* thanks the anonymous reviewers for their contribution to the peer review of this work.